Science of the Total Environment 1014 (2026) 181386

Contents lists available at ScienceDirect

Science of the Total Environment

journal homepage: www.elsevier.com/locate/scitotenv

Cross-regional characteristics, chemical composition, and source contributions of atmospheric particulate matter in Germany and India

Xiao Wang [a,*], Ramesh P. Singh [b], Elisabeth Eiche [c,d], Feng Jiang [e], Prity S. Pippal [f], Rajesh Kumar [f], Akshansha Chauhan [g], Stefan Norra [a]

[a] Institute of Environmental Sciences and Geography, Potsdam University, Potsdam, Golm, 14476, Germany
[b] School of Life and Environmental Sciences, Schmid College of Science and Technology, Chapman University, Orange, CA, 92866, USA
[c] Institute of Applied Geosciences, Karlsruhe Institute of Technology (KIT), Karlsruhe, 76131, Germany
[d] Laboratory of Environmental and Raw Materials Analysis (LERA), Institute of Applied Geosciences, Karlsruhe, 76131, Germany
[e] Institute of Meteorology and Climate Research, Karlsruhe Institute of Technology, Eggenstein-Leopoldshafen, 76344, Germany
[f] Department of Environmental Science, School of Earth Sciences, Central University of Rajasthan, Ajmer, Rajasthan, 305817, India
[g] School of Minerals and Energy Resources Engineering, University of New South Wales, Sydney, NSW, 2052, Australia

HIGHLIGHTS

- PM profiling in India and Germany via ICP-MS and 3D fluorescence
- PM in Karlsruhe from industry and traffic, in Ajmer from dust and biomass
- Highly oxygenated HULIS in Karlsruhe; less-oxygenated HULIS in Ajmer
- Integrated chemical-optical approach supports regional air-quality mitigation

GRAPHICAL ABSTRACT

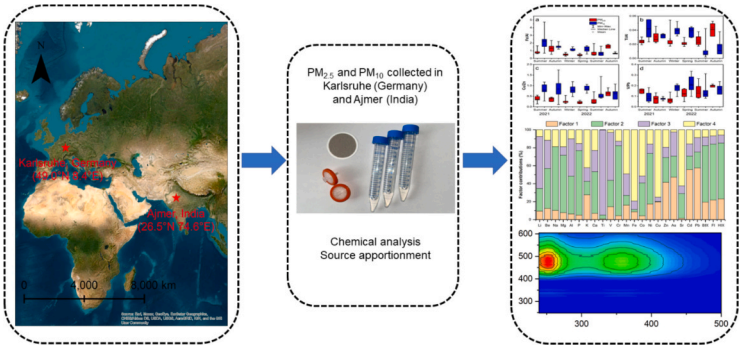

ARTICLE INFO

Keywords:
Atmospheric aerosol
Emission–excitation matrix
Humic like substances
PM
Source apportionment
Trace element

ABSTRACT

Atmospheric particulate matter (PM) influences air quality, visibility, and the radiation budget, yet inter-regional differences in sources and chemical characteristics remain poorly understood. In this study, PM samples from Karlsruhe, Germany and Ajmer, India were analyzed using inductively coupled plasma mass spectrometry (ICP-MS) and three-dimensional excitation–emission matrix fluorescence spectroscopy (3D-EEM). Elemental analysis revealed high concentrations of Na and Al were high in both locations. Elemental ratios (Fe/Al, Ti/Al, Cu/Zn, and V/Pb) reveal strong traffic- and industrial-related influences in Karlsruhe and combined dust, combustion, and industrial impacts in Ajmer. 3D-EEM analysis shows that highly oxygenated humic-like substance (HULIS) (C1 and C2) dominated in Karlsruhe (62%) during the sampling period, while less-oxygenated HULIS (C3) from biomass burning was most abundant in winter season (41%). In Ajmer, less-oxygenated HULIS remained dominant throughout the sampling period (C1, 57%), while highly oxygenated HULIS (C2) and mixed-source components (C4) contributed 19% and 2%, respectively. PMF highlighted complex source profiles, including

* Corresponding author.
E-mail address: xiao.wang@uni-potsdam.de (X. Wang).

https://doi.org/10.1016/j.scitotenv.2026.181386
Received 27 October 2025; Received in revised form 2 January 2026; Accepted 9 January 2026
Available online 15 January 2026

industrial, crustal, and mixed anthropogenic contributions in both locations. These findings improve understanding of inter-regional PM composition and sources, providing insights for targeted air quality management and climate impact assessment.

1. Introduction

Atmospheric aerosol particles are major air pollutants suspended in the atmosphere and vary widely in composition and behavior across regions. Among them, particles smaller than 10 μm (PM_{10}) and 2.5 μm ($PM_{2.5}$) receive particular attention because they can penetrate deep into the respiratory system, carry toxic components, and play an important role in atmospheric chemistry and radiative processes (Dey et al., 2004; Fuzzi et al., 2015; Kaskaoutis et al., 2012). In urban environments, PM comes from a complex mixture of natural and anthropogenic sources, such as vehicle emissions, industrial activities, biomass burning, and dust resuspension.

Understanding the sources and transformations of particulate matter is therefore essential for evaluating its environmental and health impacts. To identify PM sources, researchers typically rely on both direct and indirect approaches. Direct methods such as chemical speciation (Chen et al., 2016b), isotopic analysis (Das et al., 2018; Ray et al., 2024), and real-time measurements provide explicit evidence of emissions and are well suited for identifying short-term or event-driven pollution signals (Chen et al., 2022; Kumar et al., 2024). Indirect approaches, including receptor models (Rai et al., 2020; Siudek, 2024; Zhang et al., 2021), fluorescence spectroscopy (Chen et al., 2020; Ma et al., 2022; Rutherford et al., 2021), back-trajectory analysis (Rai et al., 2020), and chemical transport modeling (Jiang et al., 2006; Tuladhar et al., 2021; Zhang et al., 2021), help reveal broader spatial and temporal source patterns. Because each method has inherent limitations, integrating multiple, complementary techniques offers a more robust framework for source apportionment.

Although PM has been widely studied in Europe and Asia, comparative analyses across regions with contrasting climatological and socioeconomic conditions remain scarce. Such cross-regional investigations are vital for understanding how factors such as industrial structure, fuel use, meteorology, and land cover influence aerosol composition and source contributions. Germany has a temperate climate and highly developed industrial and transportation sectors, whereas India is characterized by arid to semi-arid climatic conditions, rapid urbanization, and widespread use of biomass and coal. These contrasting environmental and socioeconomic settings create fundamentally different particulate-matter source regimes.

In this study, we conduct a comparative assessment of $PM_{2.5}$ and PM_{10} collected in Karlsruhe, Germany, and Ajmer, India. By integrating elemental analysis, fluorescence spectroscopy, and receptor modeling, we (1) characterize the chemical and optical properties of PMs, (2) identify and quantify major emission sources, and (3) evaluate the regional drivers of aerosol composition in both urban settings. This multi-method approach provides a comprehensive understanding of PMs source and their variability across disparate environments, contributing to improved knowledge of urban aerosol chemistry and supporting region-tailored air-quality strategies.

2. Materials and methods

2.1. Study areas

The city of Karlsruhe is located in the southwest of Germany, the second-largest city (after Stuttgart) of Baden-Württemberg, in terms of population (about 300,000). The climate of Karlsruhe is transitional between continental and oceanic types. The historical average annual air temperature and precipitation are 10.5 °C and 770 mm. The measurement site at the Durlacher Tor is located at a central traffic junction with a three-lane road and a street crossing. Karlsruhe is located at the transition between the Rhine Valley and the northern Black Forest, a low mountain range composed mainly of gneiss and granite, overlain by red sandstone and loess deposits. The surrounding landscapes provide important ecological functions, recreational spaces, and watershed regulation. The varied geology has produced diverse soils, from fertile loess-rich deposits in the Rhine plain and Kraichgau to more acidic, less fertile soils on crystalline and sandstone substrates, shaping the region's vegetation and land use.

The city of Ajmer is located in the eastern part of Rajasthan, surrounded on three sides by the rugged Aravali hills. Ajmer has a semi-arid climate. The climate of Ajmer is dry and is subject to the extremeness of cold and heat in various places. The minimum and maximum temperatures recorded in the Ajmer district vary from 5 to 48 °C. Normal annual rainfall is 50 mm. Geologically, Ajmer lies atop the Bhilwara and Delhi Super Groups, comprising metamorphic and sedimentary formations such as gneiss and sandstone. The soils of the study areas are sandy with low water retention capacity, influencing agricultural practices. Vegetation is sparse, with approximately 6.85% of the district's area under forest cover, supporting dry deciduous species adapting to the arid conditions. Natural water bodies like Ana Sagar and Pushkar Lake are vital for the city's water supply and have cultural significance. These natural features collectively shape Ajmer's ecological and hydrological landscape. Locations of Karlsruhe, Germany and Ajmer, India are shown in Fig. 1.

2.2. Sampling

In Karlsruhe, $PM_{2.5}$ and PM_{10} samples were collected on quartz filters using a Low Volume Sampler (Comde-Derenda GmbH, Germany) from July 2021 to October 2022. The sampler was housed in a fixed weather container (49.0° N. 8.4° E) at the Durlacher Tor transport station, adjacent to the south campus of the Karlsruhe Institute of Technology (KIT). Sampling inlets were positioned 3.7 m above ground level and 1.2 m above the container roof, and the sampler operated at a flow rate of 2.3 m^3/h. A total of 71 filters of $PM_{2.5}$ and 71 filters of PM_{10} were extracted with ultrapure water and analyzed for Excitation-emission matrix (EEM) fluorescence spectra using an Aqualog spectrofluorometer (Horiba, Japan). Additionally, 37 filters of $PM_{2.5}$ and 37 filters of PM_{10} were analyzed for trace element concentrations using inductively coupled plasma mass spectrometry (ICP-MS).

In Ajmer, $PM_{2.5}$ and PM_{10} quarts samples were collected during January and June 2023 using Ecotech MicroVol-1100 Low Volume Sampler (Ecotech Pty Ltd., Australia), which was deployed on the Central University campus of Ajmer (26.5° N. 74.6° E). This instrument provides a flexible sampling platform for $PM_{2.5}$ and PM_{10} by changing the two-nozzle adaptor for $PM_{2.5}$ and PM_{10}, with flow rate flow rates of 1.0 to 4.5 L/min. The airmass reaches at the measurement site from the surrounding Thar desert, frequent long-range transport of dust, surrounding Copper and Zinc mining areas, factories and power plants depending upon the winds (S—W and N—W). A total of 20 $PM_{2.5}$ filters and 25 PM_{10} filters were extracted with ultrapure water and measured for Excitation-emission matrix (EEM) fluorescence spectra using Aqualog. Additionally, 8 filters of $PM_{2.5}$ and 8 filters of PM_{10} were analyzed for trace elements by ICP-MS. Detailed information on all samples is given in the Supplementary Materials (Table S1).

2.3. Mass concentration analysis

Every filter was weighted 3 times at different days with a

microbalance (Sartorius SE 2F, Gottingen, Germany) at a constant temperature (22 ± 3 °C) and relative humidity (35 ± 5%) prior and after sampling. The mass of $PM_{2.5}$ and PM_{10} collected on each filter was determined from the difference between pre- and post-sampling weights, and the corresponding mass concentration was calculated based on the sampled air volume.

2.4. Chemical analysis

Elemental concentration analysis was conducted using 15-mm diameter punches taken from each $PM_{2.5}$ and PM_{10} quartz filter. The filters were digested in Teflon vessels using concentrated HNO_3 (Merck, subboiled), HF (VWR, suprapur), and $HClO_4$ (VWR, normatom). The digested solutions were subsequently diluted twofold with 1% HNO_3 (subboiled) and analyzed using a high-resolution inductively coupled plasma mass spectrometer (iCap RQ, Thermo Fisher). Method detection limits (MDLs) and quantification limits (MQLs) were determined as 3σ and 10σ of procedural blanks, respectively, and all sample concentrations were blank-corrected. The analytical accuracy and precision of ICP-MS were verified using certified reference materials SRM 1648a (urban particulate matter) and GXR-2 (soil sample) from the U.S. Geological Survey (USGS, USA), with recoveries within ±10% of the certified values and relative standard deviations (RSDs) below 5%. All analyses were conducted at Institute of Applied Geosciences (AGW), Karlsruhe Institute of Technology (KIT).

2.5. Three-dimensional fluorescence spectroscopy analysis

For each $PM_{2.5}$ and PM_{10} quartz filters, 12-mm diameter punches were extracted with ultrapure water (18.2 MΩ cm) and sonicated for 30 min. Afterwards the sample solution was passed through the 0.45 μm PTFE syringe filters to remove insoluble species. Excitation and emission spectra of water-soluble organic component (WSOC) in the extracted fluids were measured by an Aqualog fluorometer (HORIBA Scientific, USA). The scanning range of the excitation wavelength was 239–500 nm and an emission wavelength were 247.0–603.5 nm. Scanning wavelength increments of excitation and emission were 3 nm and the emission wavelength increments used were 4.66 nm.

Prior to PARAFAC modeling, all fluorescence spectra were preprocessed following established procedures. Ultrapure water blanks were subtracted to remove background signals; first- and second-order Rayleigh and Raman scatter bands were removed using interpolation; and inner-filter effects were corrected using the corresponding absorbance spectra. The PARAFAC model in R program (version 4.3.3) was used to identify potential fluorescent components in WSOC (Jiang et al., 2022; Murphy et al., 2013; Pucher et al., 2019).

2.6. Fluorescence indices analysis

The humification index (HIX), fluorescence index (FI), and biological index (BIX) were calculated, reflecting the degree of humification or aromaticity, the source of organic matter, and the contribution of recently produced biological material (Dey et al., 2021). The three fluorescence indices (HIX, FI, and BIX) are given by the following equations (Huguet et al., 2009):

$$HIX = \frac{F(E_x = 254\ nm, E_m = 435 - 480\ nm}{F(E_X = 254\ nm, E_m = 300 - 345\ nm)} \quad (1)$$

$$FI = \frac{F(E_X = 370\ nm, E_m = 450\ nm)}{F(E_x = 370\ nm, E_m = 500\ nm)} \quad (2)$$

$$BIX = \frac{F(E_X = 310\ nm, E_m = 380\ nm)}{F(E_x = 310\ nm, E_m = 430\ nm)} \quad (3)$$

where F is the fluorescence intensity, E_x and E_m are the excitation and emission wavelengths. E_m of HIX was determined in the range of 435–480 and 300–345 nm using eq. (1).

2.7. Positive matrix factorization analysis

Positive Matrix Factorization (PMF) is a receptor modeling technique widely used for source apportionment of atmospheric particulate matter. It decomposes a matrix of observed data (typically chemical species concentrations) into two non-negative matrices: factor contributions and factor profiles. By applying a weighted least squares approach that accounts for the uncertainties in the data, PMF minimizes the residuals between observed and modeled concentrations. Unlike traditional factor analysis methods, PMF imposes non-negativity constraints, ensuring physically meaningful results. This model is particularly effective in identifying and quantifying pollution sources without prior knowledge of source profiles, making it a robust tool in environmental studies. PMF diagnostics indicated that the model solution was robust, with consistent Q/Qexp ratios and stable factor profiles across multiple runs. Bootstrap and Kolmogorov-Smirnov (KS) tests further confirmed the reliability of

Fig. 1. Locations of Karlsruhe, Germany and Ajmer, India.

the factor contributions and profiles.

3. Results and discussion

3.1. Elemental concentration

The elemental concentration profiles of $PM_{2.5}$ and PM_{10} in Karlsruhe and Ajmer are shown in Table 1. The trace elements in $PM_{2.5}$ and PM_{10} at Karlsruhe and Ajmer show distinct distribution patterns. In Karlsruhe, Na (4207 ± 2245 ng/m^3 in $PM_{2.5}$; 2785 ± 1005 in PM_{10}), Ca (1887 ± 1233 ng/m^3; 1518 ± 717 ng/m^3), and Al (853 ± 556 ng/m^3; 775 ± 369 ng/m^3) dominate, while trace metals like Be (0.04 ± 0.03 ng/m^3; 0.03 ± 0.02 ng/m^3) and Co (0.36 ± 0.39 ng/m^3; 0.26 ± 0.25 ng/m^3) are minimal. In contrast, samples from Ajmer exhibits significantly higher concentrations of Na (16,586 ± 28,975 ng/m^3 in $PM_{2.5}$; 5263 ± 1419 ng/m^3 in PM_{10}), and Al (4647 ± 3984 ng/m^3; 3812 ± 965 ng/m^3), while trace metals like V (0.51 ± 0.28 ng/m^3; 0.54 ± 0.18 ng/m^3) and Co (0.14 ± 0.12 ng/m^3; 0.11 ± 0.04 ng/m^3) are lower.

The concentrations of heavy metals such as Pb were similar in $PM_{2.5}$ measured at Ajmer (16.5 ± 15.6 ng/m^3) and Karlsruhe (10.9 ± 9.24 ng/m^3), whereas Cd concentrations Ajmer (1.06 ± 0.65 ng/m^3) in Ajmer $PM_{2.5}$ were found to be higher compared to those in Karlsruhe (0.27 ± 0.23 ng/m^3). Titanium (Ti) concentrations in $PM_{2.5}$ were found to be comparable at both the locations (Ajmer: 35.5 ± 14.6 ng/m^3, Karlsruhe: 37.6 ± 77.0 ng/m^3).

3.2. Source apportionment for PM and variation of elemental ratio

3.2.1. Elemental ratios

In atmospheric particulate matter ($PM_{2.5}$ and PM_{10}), Fe and Al are generally indicators of crustal/soil (dust) inputs and resuspended road/construction dust, emissions from coal-based power plants and brick kilns (Prasad et al., 2006; Sharma and Mandal, 2023). Titanium is often regarded as a relatively conservative lithogenic tracer in aerosols because it is typically bound in refractory minerals and less prone to chemical alteration (Hird et al., 2024). Cu and Zn are commonly associated with anthropogenic sources—especially traffic-related non-exhaust emissions (tire and brake wear) and various industrial/metal-working activities (Jeong et al., 2022). Vanadium (V) is a tracer of heavy fuel and oil combustion, including emissions from ships and some industrial sources. Lead (Pb) has historically been associated with gasoline and metallurgical or industrial sources; today, it primarily reflects industrial and metal-processing emissions where present (Das et al., 2018). Element ratios are used in source apportionment studies and reduce the influence of absolute concentration variability and thus provide more robust and reliable markers for source identification. In this study, the ratios of Fe/Al, Ti/Al, Cu/Zn and V/Pb are used at the sampling sites to identify the source.

Table 1
Elements concentrations (mean ± SD ng/m^3) of $PM_{2.5}$ and PM_{10} in Karlsruhe and Ajmer.

Element	$PM_{2.5}$		PM_{10}	
	Karlsruhe	Ajmer	Karlsruhe	Ajmer
Li	0.56 ± 0.50	3.00 ± 2.87	2.74 ± 2.53	2.23 ± 0.58
Be	0.04 ± 0.03	–	0.03 ± 0.02	–
Na	4207 ± 2245	16,587 ± 28,975	2785 ± 1005	5263 ± 1419
Mg	823 ± 453	2849 ± 6295	554 ± 214	330 ± 129
Al	853 ± 556	4647 ± 3984	775 ± 369	3812 ± 965
P	96.2 ± 60.0	–	96.3 ± 52.0	–
K	705 ± 692	2595 ± 1145	536 ± 355	2608 ± 696
Ca	1887 ± 1233	7225 ± 11,925	1518 ± 717	3084 ± 1037
Ti	37.6 ± 77.0	35.5 ± 14.6	27.0 ± 22.0	36.6 ± 9.30
V	1.18 ± 0.95	0.51 ± 0.28	1.15 ± 0.67	0.54 ± 0.18
Cr	18.4 ± 19.2	1.92 ± 1.68	12.0 ± 9.47	1.49 ± 0.51
Mn	16.6 ± 16.8	5.11 ± 4.55	18.6 ± 14.7	3.25 ± 1.27
Fe	785 ± 961	143 ± 105	1059 ± 1008	127 ± 46.2
Co	0.36 ± 0.39	0.14 ± 0.12	0.26 ± 0.25	0.11 ± 0.04
Ni	17.4 ± 18.7	–	9.36 ± 9.95	–
Cu	20.0 ± 23.8	2.85 ± 2.74	27.2 ± 27.1	1.61 ± 1.17
Zn	57.1 ± 47.8	2644 ± 1593	34.5 ± 24.1	4030 ± 1058
As	0.87 ± 0.73	4.85 ± 4.66	0.72 ± 0.45	8.40 ± 4.03
Sr	7.54 ± 11.2	63.2 ± 29.2	4.75 ± 3.25	90.7 ± 24.4
Cd	0.27 ± 0.23	1.06 ± 0.65	0.19 ± 0.13	0.56 ± 0.52
Pb	10.9 ± 9.24	16.5 ± 15.6	8.38 ± 5.20	9.28 ± 6.18

The Fe/Al and Ti/Al ratio are commonly used as indicators of crustal and/or soil-derived sources. In Karlsruhe (Fig. 2), Fe/Al ratio in PM_{10} consistently exhibited higher mean ratios than $PM_{2.5}$ across seasons, with the highest PM_{10} average value (2.34 ± 1.51) during summer 2021 and the lowest (0.69 ± 0.13) during autumn 2022. The $PM_{2.5}$ Fe/Al ratio in Karlsruhe shows large variations. The maximum is observed during autumn 2021 (1.34 ± 0.69) and low values during winter 2021 (0.50 ± 0.16). The average Fe/Al ratio observed in $PM_{2.5}$ (0.83 ± 0.55) and PM_{10} (1.26 ± 0.78) in Karlsruhe are found to be higher compared to the Upper Continental Crust (UCC) (0.43) (Taylor and McLennan, 1985). Karlsruhe lies within the Upper Rhine Plain; a region composed mostly of alluvial and loess quaternary sediments which would be expected to yield Fe/Al ratios close to or below UCC values under non-polluted conditions. While the city hosts diverse industrial activities, including machinery and automotive manufacturing, a large industrial harbor, and nearby metallurgical facilities. Taken together, the elevated Fe/Al ratios in the PM_{10} fraction and their seasonal maxima indicate that these particles are primarily derived from industrial emissions, road dust resuspension, and mechanical abrasion, including tire and brake wear. In contrast, lower $PM_{2.5}$ Fe/Al ratios indicate a larger proportion of combustion and fine industrial sources. The Fe/Al ratios observed in both $PM_{2.5}$ (0.0345 ± 0.0238) and PM_{10} (0.0330 ± 0.0072) in Ajmer are notably lower than those typically found in crustal materials, such as UCC ratio of 0.43 (Taylor and McLennan, 1985). Ajmer, located in the semi-arid region of Rajasthan, experiences seasonal variations in wind patterns and temperature, which can significantly influence the dispersion and transport of particulate matter. During the winter season, wind in Ajmer predominantly flows from the N—W, W, and S—W directions; in summer, it shifts to W, S—W, and S directions with speeds of 1–2 m/s. During the monsoon season, the winds are mainly westerly (1.6 m/s), and the average wind speed is higher compared to winter (0.97 m/s) and summer (1.2 m/s) (Fig. S1). These meteorological conditions may affect both the regional transport of dust and the dispersion of local emissions, thereby shaping the observed elemental composition. The city's industrial activities, including brick kilns and small-scale manufacturing, along with vehicular emissions, are likely contributors to the observed elemental composition.

In Karlsruhe, the Ti/Al ratios were 0.042 ± 0.01 for $PM_{2.5}$ and 0.031 ± 0.015 for PM_{10}, while in Ajmer the corresponding values were 0.0091 ± 0.0038 for $PM_{2.5}$ and 0.0096 ± 0.0006 for PM_{10}. Compared to UCC reference ratio of ~0.05 (Wedepohl, 1995), all Ti/Al values are significantly lower. This strong depletion of Ti relative to Al indicates that the particulate matter is not dominated by soil or crustal erosion but rather influenced by anthropogenic sources such as traffic emissions, construction, and road dust, and industrial or combustion-related particles, all of which can contribute to Al enrichment (Shelley et al., 2015; Zhang et al., 2020).

In Karlsruhe, Cu/Zn ratios in PM_{10} were generally higher than in $PM_{2.5}$, peaking in winter 2021 (1.19) but exhibiting large seasonal fluctuations, as evidenced by extreme PM_{10} values (e.g., maximum 1.75 in autumn 2021). $PM_{2.5}$ Cu/Zn ratios stabilized in 2022, except for a spike in autumn (0.69). The mean Cu/Zn ratios of $PM_{2.5}$ and PM_{10} are 0.33 ± 0.19 and 0.77 ± 0.33 respectively. The sampling site was located at a busy intersection, adjacent to both tram stop and bus station. The relatively higher ratio in PM_{10} indicates a potential contribution of Cu from traffic-related non-exhaust emissions, including brake and tire wear (Siudek, 2024; Viana et al., 2008). However, the generally lower ratios suggest that Zn-dominated sources, rather than Cu-enriched traffic emissions, are the primary contributors. In Ajmer, The Cu/Zn

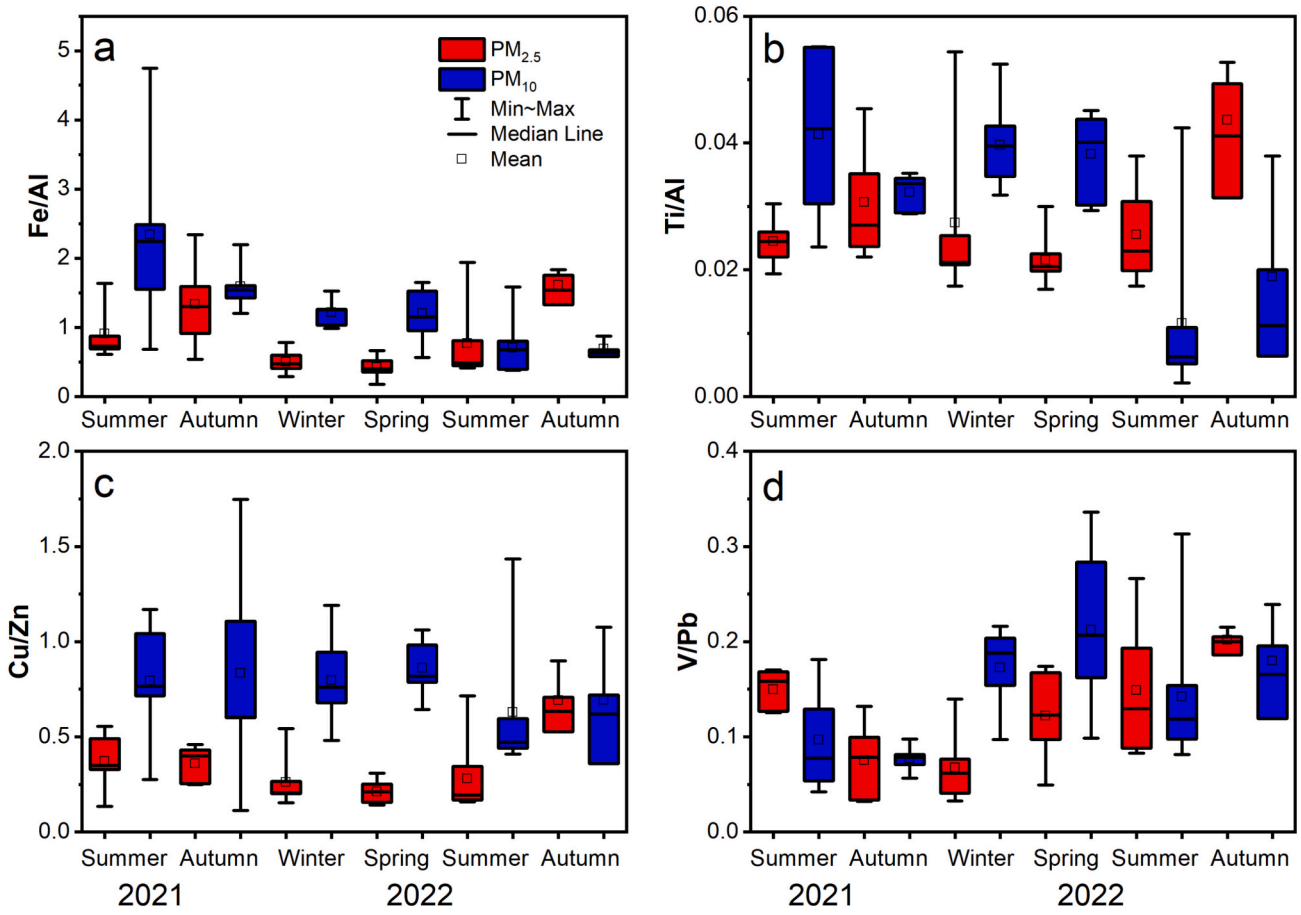

Fig. 2. Seasonal variations of elemental ratio for Fe/Al (a), Ti/Al (b), Cu/Zn (c) and V/Pb (d) measured in Karlsruhe.

ratio substantially differs between $PM_{2.5}$ (0.0137 ± 0.0250) and PM_{10} (0.0004 ± 0.0002). The much lower value in PM_{10} suggests that Zn may be more enriched in the coarser fraction, due to wear and tear from brake pads, tire abrasion, and industrial emissions. The elevated Cu/Zn ratio in $PM_{2.5}$ is due to the fine particulate emissions from combustion processes, such as vehicle exhaust and industrial smelting (Siudek, 2024).

In Karlsruhe, the V/Pb ratio was higher in 2021 than in 2022 for both $PM_{2.5}$ and PM_{10}, while the $PM_{2.5}$ ratio in 2022 gradually increased, peaking at 0.20 in autumn. Seasonal shifts were pronounced for V/Pb, particularly in PM_{10}, where winter 2021 shows the highest average values (0.17) and the maximum season value (0.34). The V/Pb ratio, a well-established tracer for coal combustion (V/Pb > 1), traffic emissions (V/Pb < 1), and industrial discharges (V/Pb ≪ 1), is 0.12 for $PM_{2.5}$ and 0.15 for PM_{10} in Karlsruhe. These values, which are both less than 1, suggest that the primary sources of particulate matter are vehicular emissions and industrial emissions. The V/Pb ratio in Ajmer is lower in $PM_{2.5}$ (0.0470 ± 0.0364) and PM_{10} (0.0777 ± 0.0401) (Table 2), which may indicate industrial emissions (Das et al., 2018).

Table 2
Elemental ratios for Fe/Al, Ti/Al, Cu/Zn and V/Pb in Ajmer.

Elemental Ratio	$PM_{2.5}$	PM_{10}
Fe/Al	0.0345 ± 0.0238	0.0330 ± 0.0072
Ti/Al	0.0091 ± 0.0038	0.0096 ± 0.0006
Cu/Zn	0.0137 ± 0.0245	0.0004 ± 0.0002
V/Pb	0.0470 ± 0.0364	0.0777 ± 0.0401

Note: We selected eight $PM_{2.5}$ and eight PM_{10} samples from Ajmer for ICP-MS analysis, covering different seasons. The element ratio results showed little variation compared to samples from Karlsruhe and UCC. Therefore, we focus only on the average element ratio value analysis of the Ajmer samples.

3.2.2. *Fluorescence indices analysis*

An overview of fluorescence indices for each sample and comparison of the Humification Index (HIX) with the Fluorescence Index (FI) and the Biological Index (BIX) are shown in Fig. S2–S4 and in Table 3. HIX is strongly influenced by the aromaticity and the decreases in the hydrogen-to-carbon ratio during humification and is indirectly related to the mineralization rate (Hansen et al., 2016; Xu et al., 2021). In Karlsruhe, the average HIX value of $PM_{2.5}$ and PM_{10} are 0.72 ± 0.13 and 0.77 ± 0.06 respectively and in Ajmer, 0.69 ± 0.08 and 0.68 ± 0.10 respectively, which are lower than Mohanpur city, India (0.93 ± 0.03) (Dey et al., 2021) and control SOA (Secondary organic aerosols) (2.30 ± 1.50) (Lee et al., 2013). These observations suggest a low mineralization rate, C/H ratio and aromatic compound concentrations and thus show less impact from allochthonous sources, such as biomass and animal manure.

FI and BIX are used to distinguish WSOC derived from terrestrial sources or microbial sources. If the BIX (FI) value is below 0.6 (1.4), it suggests terrestrial-derived organic matters; if the BIX (FI) value is more than 1.0 (1.9), microbial-derived organic matter is suggested (Xu et al., 2021). In Karlsruhe, the average FI values of $PM_{2.5}$ and PM_{10} are 1.34 and 1.32 respectively, and the average BIX values of $PM_{2.5}$ and PM_{10} are 0.85 and 0.84 respectively. These BIX and FI values suggest that the fluorescent components of water-soluble organic aerosols in Karlsruhe are primarily influenced by a combination of terrestrial and microbial sources. In Ajmer, the average FI value of $PM_{2.5}$ and PM_{10} are 1.30 and 1.29 respectively. The average BIX values of $PM_{2.5}$ and PM_{10} are 0.85 and 0.82 respectively. BIX and FI values of $PM_{2.5}$ and PM_{10} in Ajmer were mainly distributed within terrestrial and microbial dominated

Table 3
Fluorescence indices of the WSOC in Karlsruhe and Ajmer.

City	Period	$PM_{2.5}$			PM_{10}		
		HIX	FI	BIX	HIX	FI	BIX
Karlsruhe	Spring	0.76 ± 0.08	1.32 ± 0.10	0.85 ± 0.04	0.81 ± 0.02	1.31 ± 0.03	0.81 ± 0.04
	Summer	0.61 ± 0.20	1.27 ± 0.24	0.83 ± 0.10	0.72 ± 0.10	1.30 ± 0.09	0.85 ± 0.07
	Autumn	0.77 ± 0.02	1.43 ± 0.09	0.88 ± 0.04	0.79 ± 0.02	1.34 ± 0.05	0.86 ± 0.05
	Winter	0.75 ± 0.03	1.35 ± 0.04	0.92 ± 0.03	0.77 ± 0.02	1.29 ± 0.02	0.92 ± 0.04
	Heating period	0.77 ± 0.03	1.37 ± 0.07	0.90 ± 0.04	0.78 ± 0.02	1.31 ± 0.04	0.89 ± 0.05
	Non-heating period	0.69 ± 0.16	1.32 ± 0.19	0.83 ± 0.08	0.76 ± 0.08	1.32 ± 0.07	0.82 ± 0.06
	Daytime	0.38 ± 0.10	1.20 ± 0.16	0.92 ± 0.08	0.62 ± 0.06	1.23 ± 0.08	0.85 ± 0.02
	Night	0.45 ± 0.07	0.98 ± 0.23	0.75 ± 0.14	0.66 ± 0.07	1.28 ± 0.12	0.92 ± 0.06
	Daily	0.80 ± 0.03	1.32 ± 0.03	0.86 ± 0.06	0.79 ± 0.07	1.35 ± 0.06	0.85 ± 0.08
	Total	0.72 ± 0.13	1.34 ± 0.16	0.85 ± 0.07	0.77 ± 0.06	1.32 ± 0.06	0.84 ± 0.06
Ajmer	Winter	0.75 ± 0.05	1.37 ± 0.08	0.88 ± 0.11	0.78 ± 0.03	1.33 ± 0.05	0.84 ± 0.08
	Summer	0.70 ± 0.07	1.31 ± 0.12	0.81 ± 0.10	0.67 ± 0.11	1.30 ± 0.15	0.83 ± 0.06
	Monsoon period	0.62 ± 0.06	1.19 ± 0.15	0.88 ± 0.10	0.63 ± 0.07	1.25 ± 0.09	0.79 ± 0.07
	Total	0.69 ± 0.08	1.30 ± 0.14	0.85 ± 0.11	0.68 ± 0.10	1.29 ± 0.12	0.82 ± 0.07

areas.

In Karlsruhe, the HIX, FI, and BIX values of $PM_{2.5}$ remain relatively low. Noticeable variations are observed during the daily resolved sampling period (Sample IDs 44–53). This period is characterized by shorter daytime and nighttime sampling durations compared with other sampling periods in Karlsruhe, which may contribute to the greater variability in these optical indices. In the summer season, southwest winds dominate in Karlsruhe (Fig. S5–S7), the sampling point is located at an X-shaped road intersection, forming an air duct that supports the diffusion of pollutants. $PM_{2.5}$ and PM_{10} HIX values during daytime are lower compared to nighttime (Table 3). We have observed that building and road construction emissions are higher during daytime observations, suggesting the lower HIX value is influenced by natural aerosols and local activities. $PM_{2.5}$ and PM_{10} HIX values during winter season are higher compared to summer season, could be due to heating combustion (Dong et al., 2024).

3.2.3. *Chromophores identification*

Fig. 3 shows some specific fluorescence components, three different basic substances (Highly oxygenated species, less-oxygenated species/terrestrial origin and Protein-like and non-N-containing species (the letter A–C shown in Fig. 3)) identified and classified by the chromophores of the WSOC in submicron aerosols (Chen et al., 2016a). 11 specific substances such as woodsmoke species, soil and sand substances are marked in Fig. 3.

For the samples from Karlsruhe, 4 different fluorescence components are identified from the EEM-PARAFAC model (Fig. 4). Two peak values of fluorophore were identified in C1, the primary fluorescence peak at <240 nm (Ex) and 408 nm (Em), and the secondary fluorescent peak at 323 nm (Ex) and 408 nm (Em). C1 can be identified as highly oxygenated HULIS component (Jiang et al., 2022).

C2 shows two peaks of fluorophore. The ranges of excitation (Ex) and emission (Em) wavelengths of C2 are larger than those of C1. The

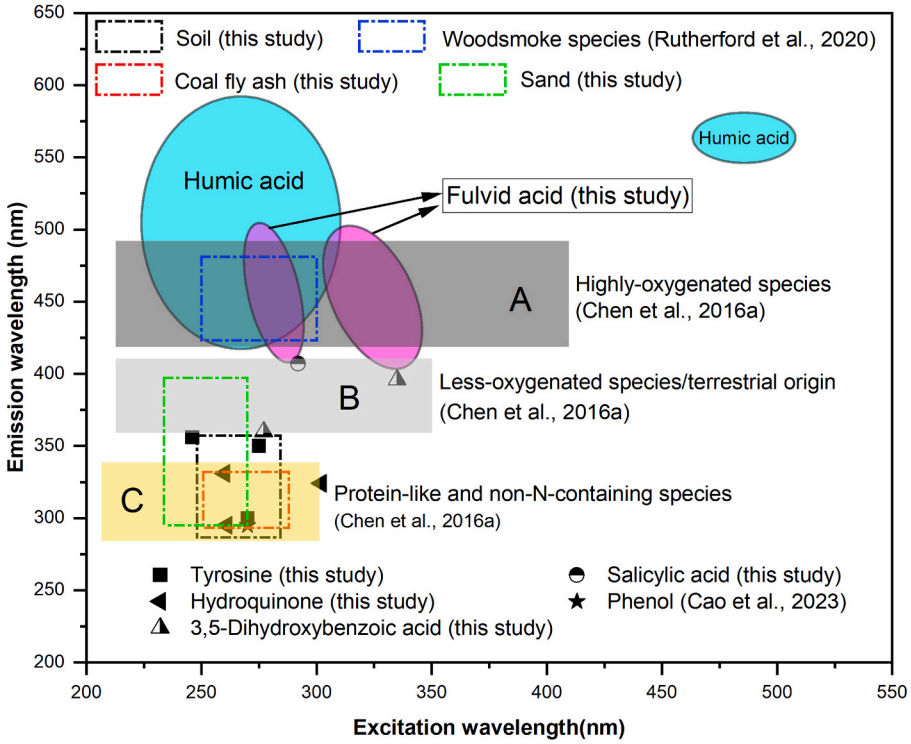

Fig. 3. Summary of the fluorescence component identified in previous (Cao et al., 2023; Chen et al., 2016a; Rutherford et al., 2020) research and in this study. A–C stands highly oxygenated species, less-oxygenated species/terrestrial origin and protein-like and non-N-containing species, respectively, which are 3 basic components.

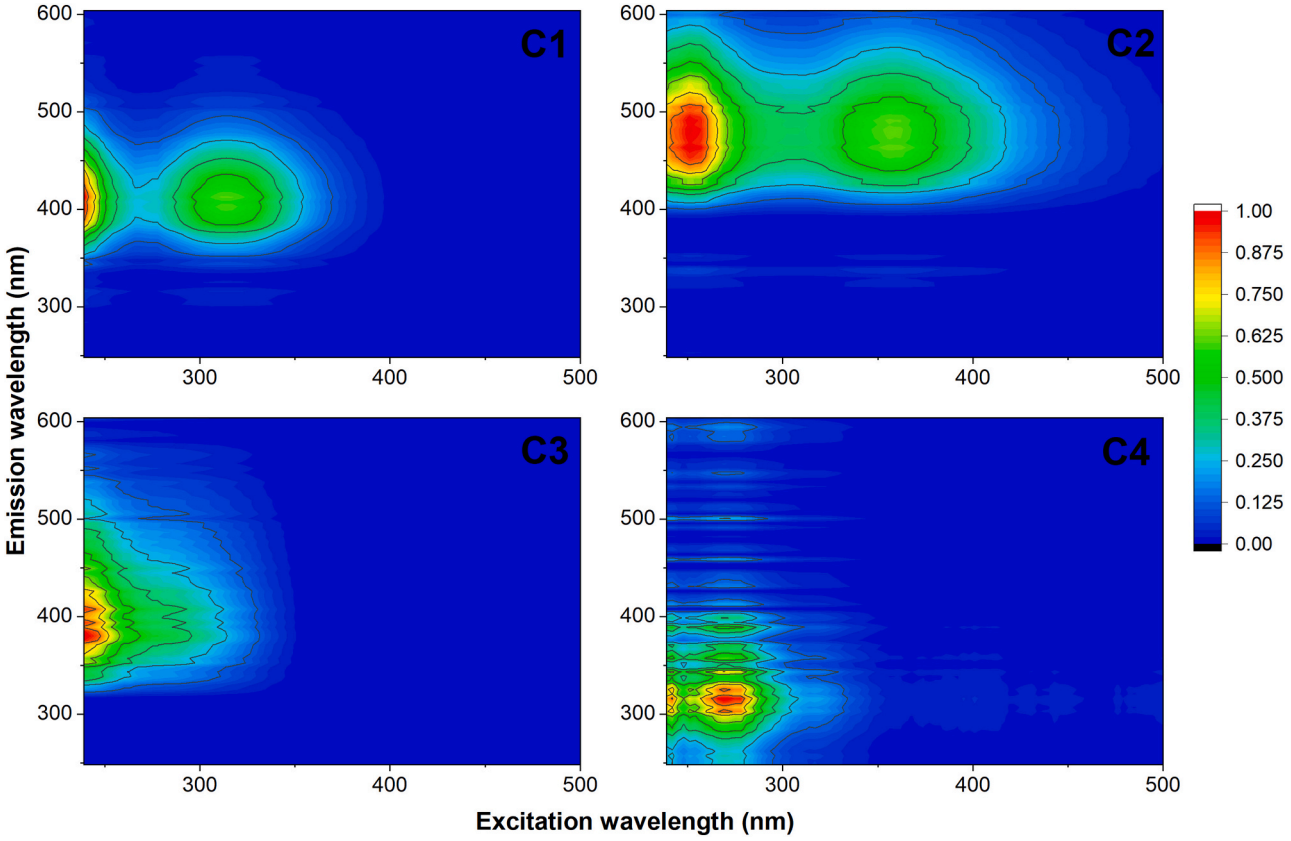

Fig. 4. Four different fluorescence components identified by EEM-PARAFAC model of the samples from Karlsruhe (Germany). C1 and C2: Highly oxygenated HULIS component, C3: Biomass burning with less-oxygenated HULIS component, and C4: Phenol- and naphthalene-like component.

primary fluorescent peak of C2 occurs at 248 nm (Ex) and 469 nm (Em). The secondary fluorescent peak occurs at 362 nm (Ex) and 469 nm (Em). These peaks can be classified as highly oxygenated HULIS component.

The peak value fluorophore at <240 (Ex) and 363 nm (Em) observed in C3 stands for biomass burning with less-oxygenated HULIS components. Four fluorescence peaks are observed of C4, the first fluorescence peak at 242 nm (Ex) and 311 nm (Em) is related to aromatic acid substances (such as phthalic acid, trimesic acid) and phenolic compounds (4-Hydroxyacetophenone and Vanillin) (Cao et al., 2023). The excitation and emission wavelength of the second fluorescence peak varies between 260 and 290 nm and 290–330 nm. Three 3 peaks are visible, the main peak at 269 nm (Ex) and 311 nm (Em) and two sub peaks at 269 nm (Ex) /305 nm (Em) and 269 nm (Ex) /325 nm (Em), respectively. These peaks can be associated with phenol- and naphthalene-like components. The third fluorescence peak at 275 nm (Ex) and 343 nm (Em) and the fourth fluorescence peak at 275 nm (Ex) and 369 nm (Em are similar with the dust substances (275 nm (Ex) and 369 nm (Em)) sampled in South Korea. In this research they represent ultra and low molecular weight organic matter of anthropogenic input (Aryal et al., 2015; Fu et al., 2010). Based on the above, C4 substances are inferred to originate from multiple sources, indicating mixed origins.

Four different fluorescence components were identified by EEM-PARAFAC model of the samples from Ajmer (Fig. 5) as well. Two peak values of fluorophore identified in C1, the primary fluorescent peak at <240 nm (Ex) and 384 nm (Em), and the secondary fluorescent peak at 299 nm (Ex) and 384 nm (Em), which is associated with biomass burning with less-oxygenated HULIS component.

The excitation and emission wavelength of C2 varies 240–400 nm and 400–550 nm and 2 fluorescence peaks were observed of C2. The first peak at 251 nm (Ex) and 472 nm (Em), which is associated with highly oxygenated HULIS component (Jiang et al., 2022). The second peak value at 353 nm (Ex) and 472 nm (Em), is similar with WSOC in Godavari, Nepal (Table S2) (Wu et al., 2019) considered as the Humic-like component. C3 peak value at 269 nm (Ex) and 302 nm (Em), is considered as Protein-like component (Chen et al., 2016a).

C4 peak value at 374 nm (Ex) and 357 nm (Em), which is associated with microbial metabolic by-products, aromatic substances, and other functional groups containing more carbonyl and carboxyl groups and HULIS substances (Cao et al., 2023; Sciscenko et al., 2022; Wang et al., 2022; Wu et al., 2017), we consider that C4 to be the substances from multiple mixed sources (Cao et al., 2023).

In Fig. 6, the relative contribution of the identified chromophore components of Karlsruhe is shown for different seasons. Highly oxygenated HULIS components (C1 and C2) dominated with 63% during spring season, 70% in summer, 59% in autumn, 48% in winter seasons, 53% during heating period and 68% in non-heating periods, respectively. These high fractions likely reflect dominant secondary formation (extensive photochemical and aqueous-phase oxidation of VOCs) and may be further enhanced by anthropogenic precursors from the surrounding industrial infrastructure. The Karlsruhe region hosts multiple large-scale energy, petrochemical, metal-processing, and manufacturing facilities, as well as major tire and electrical engineering production sites, which emit substantial amounts of VOCs, SO_2, and NOx. Emissions from these combined industrial activities can promote SOA formation and aging during atmospheric transport, particularly under favorable meteorological conditions. Biomass burning, including less-oxygenated HULIS component (C3) has a high relative contribution of 41% in winter, but a low contribution of 10% during summer season. The contribution of C3 during spring and autumn seasons is roughly equivalent, at 27% and 30%, respectively. The relative C3 contribution in the heating period (38%) is about 2.5 times higher than in non-heating period (15%), suggesting a significant influence by biomass combustion emissions such as heating. The phenol- and naphthalene-like components (C4) contributed 10% in spring, 20% in summer, 11% in

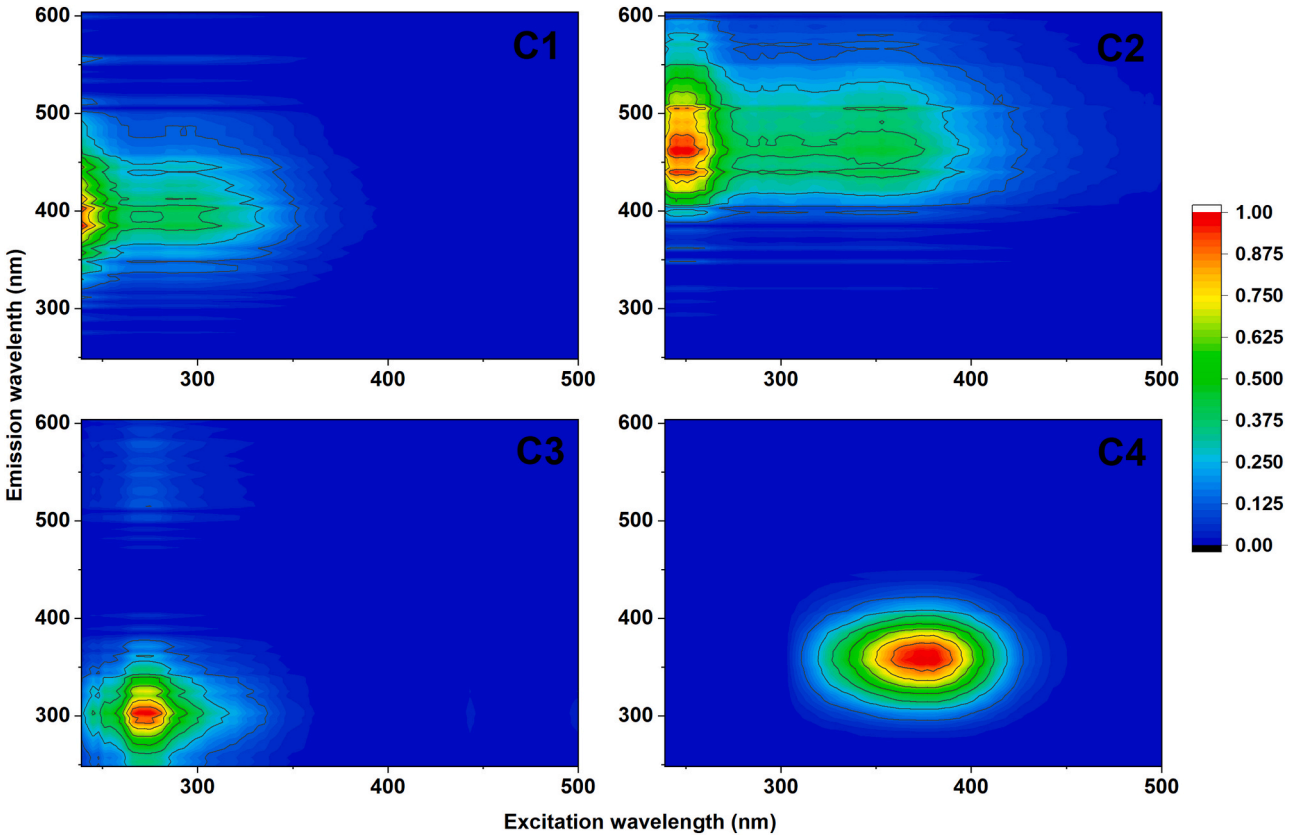

Fig. 5. Different fluorescence shows four components identified using EEM-PARAFAC model of the samples from Ajmer (India). C1: Biomass burning with less-oxygenated HULIS component, C2: Highly oxygenated HULIS component, C3: Protein-like component, and C4: Multiple mixed sources substances.

autumn and 10% in winter, respectively. Compared with other components, C4 shows only lower contributions and relatively stable trend of change in the four seasons. C4 contribution in the non-heating period (17%) is about 1.8 times higher than in heating period. Relative contribution of C1–C4 in daytime are similar with at night (Fig. 6).

Fig. S8 (a) shows the contributions of every sample from $PM_{2.5}$ of Karlsruhe, the relative concentration of C1 decreased from summer to winter, reaching the lowest contribution in winter (end of 2021 and beginning of 2022), then increased from winter to summer, reaching the highest contribution in summer. C2 shows a relatively stable contribution throughout the different seasons. The C3 content is increasing from autumn to winter then decreasing from winter to spring, which also suggested C3 was from the biomass burning or other combustion sources. There was no measurable contribution of C3 for samples ID 48 to 49 and 51 to 52. The contributions of C4 are significant for samples ID 46 to 52, ID 46 has the highest contribution (60%) to total fluorescence intensity.

The relative contributions of PM_{10} at Karlsruhe are shown in Fig. S8 (b) for different seasons of 2021 and 2022. The C1 share is similar with the $PM_{2.5}$ samples, with a substantial contribution in summer and a slightly lower in winter. The contribution of C2 does not vary significantly in different samples and seasons. C3 has a substantial contribution in winter and has a bright influence in spring and autumn. The contribution of C4 is small and the variation is not significant in different seasons. We found that the contribution of C4 was higher in sample IDs 44 to 53 (the daytime samples, night samples and the whole day samples).

The relative contribution of the four different chromophore components in Ajmer is shown in Fig. 7. The share of less-oxygenated HULIS components (C1) dominates 65%, 55%, 57% and 57% during winter, summer, monsoon seasons, and the whole period, respectively. Coal is the main fuel used in this area (Sharma, 2020), which contributed more than half of the contribution to the component. Highly oxygenated HULIS component (C2) is present with a share of dominated 24% during winter, 19% summer, 16% in the monsoon season and 19% in the whole sampling period. The C2 contribution during the monsoon is lower compared to winter and summer seasons. Highly oxygenated HULIS components are likely influenced by terrestrial dust and local biogenic sources. Ajmer is surrounded by desert areas to the north and west. During winter and summer, the climate is generally dry, with prevailing west, southwest, and northwest winds (Fig. S1), suggesting that some particulate matter could be transported from the western desert. In contrast, the monsoon season brings increased precipitation, which may enhance particle deposition and reduce the contribution of desert dust to the city. The relative contribution of the protein-like component (C3) is higher during the monsoon (26%) than in winter (12%) and summer (22%), which could reflect enhanced local biological activity or secondary organic matter formation under more humid conditions. Multiple mixed-source substances (C4) account for 4% in summer, 0.4% in the monsoon, and 2% over the whole year, indicating a minor but persistent influence from various anthropogenic or mixed sources. Overall, these results suggest seasonal variability in HULIS composition, but further source apportionment and quantitative analyses would be required to robustly identify the dominant sources.

3.2.4. *Result of positive matrix factorization analysis*

Fig. 8 shows the factor contributions (%) of elements and EEM fluorescence indices (HIX, FI, BIX) of $PM_{2.5}$ and PM_{10} in Karlsruhe, based on the PMF model. Factor 1 plays a major role for elements such as Zn, As, Cd, and Pb, potentially reflecting inputs from industrial sources. Factor 2 appears to be decisive for most elements, particularly for Na, Mg, Al, P, Cr Ni, Zn, and the fluorescence indices (HIX, FI, BIX), accounting for a major fraction of the variance. This suggests that Factor 2 likely represents a mixed source, dominated by crustal or resuspended

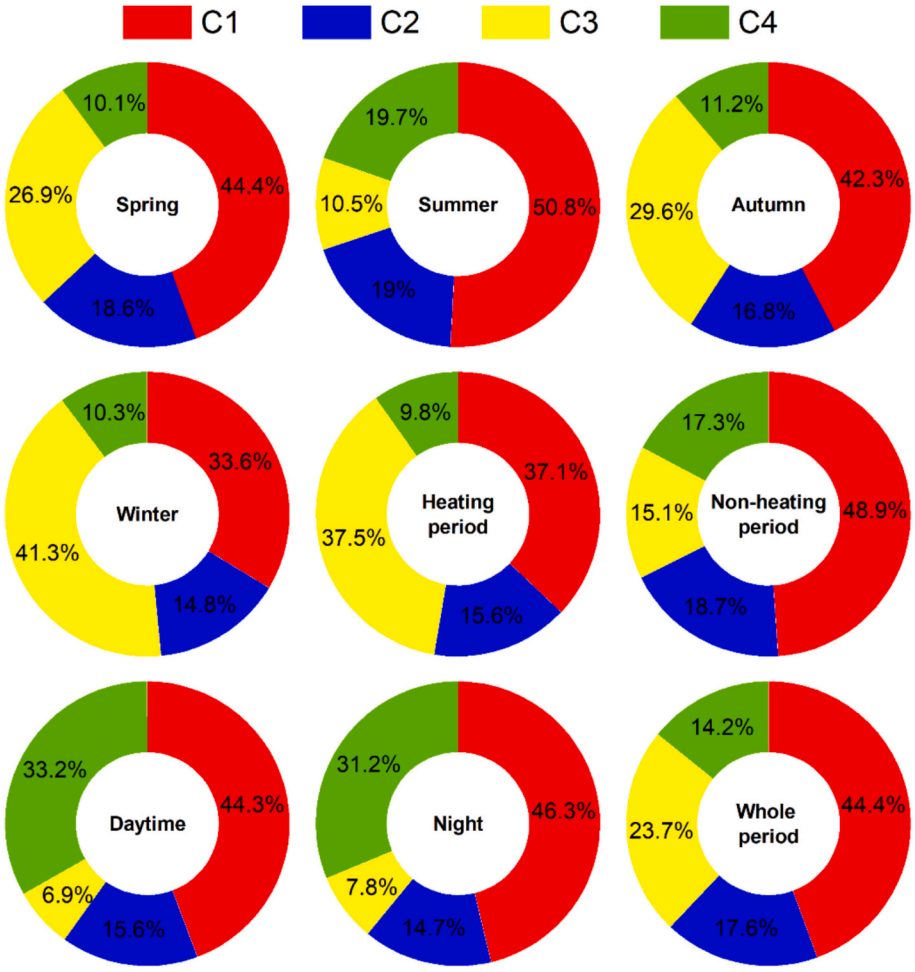

Fig. 6. Relative contributions of 4 PARAFAC-derived chromophore components for $PM_{2.5}$ and PM_{10} in Karlsruhe during different sampling periods.

dust (Al, Mg), with contributions from industrial and traffic emissions (Ni, Zn, Na), as well as biomass burning and secondary organic matter (P, HIX/BIX).

Factor 3 has a moderate contribution across multiple elements, particularly in Li, Ti, Al, and V, suggesting a potential source related primarily to crustal materials such as soil dust/windblown dust, as indicated by the presence of Al and Ti. The presence of V, commonly associated with heavy oil combustion or industrial emissions, may indicate an anthropogenic contribution. Potential minor contributions from natural sources cannot be excluded, although further source apportionment would be required to confirm this. Factor 4 shows substantial contributions from K, Mn, Fe, Co, Cu, and Sr. This pattern suggests a co-varying signal influenced by multiple activities rather than a single dominant source. While K and Mn are often linked to biomass burning, they may also arise from high-temperature industrial combustion processes such as those occurring in petroleum refining and energy production. In contrast, Fe, Co, Cu, and Sr are more typically related to industrial or metal-processing activities. Considering that Karlsruhe hosts petroleum refining, energy generation, metal recycling and processing, and various manufacturing sectors, the composition of Factor 4 is consistent with overlapping contributions from both combustion-related and industrial emissions in this complex urban environment.

The results show distinct factors that govern the distributions of the analyzed elements and EEM fluorescence indices, implying a complex interplay of natural and anthropogenic influences. The dominance of Factor 2 for the fluorescence indices suggests a significant association with organic matter characteristics and potential biogeochemical processes. Further interpretation of these factors could provide insights into the sources and transport mechanisms of trace elements and dissolved organic matter in the studied system.

In Ajmer, factor 1, has a strong contribution of elements like Li, K, Ti, Fe, Zn, Cd and BIX (Fig. 9). These are commonly associated with local lithophile and long-range transport sources (Singh et al., 2008). Factor 2, which is primarily dominated by elements such as Na, Mg and Ca, suggests geogenic sources. These elements are typically derived from soil/sand dust, mineral weathering, and the geogenic part of resuspended road dust. Factor 3, which is strongly associated with elements such as Zn, As, V, Sr and FI, shows a mixed source of industrial emissions and biomass burning. The presence of Zn and as suggestion influences metal smelting, coal combustion, and waste incineration. The Rajasthan province is very rich in different kinds of metals mines such as Copper, Zinc, Lead etc. (Jain et al., 2022; Yadav and Rajamani, 2005), these mines are about 90 km from Ajmer. At the measurement site in Ajmer, dust is prevalent during the pre-monsoon season. In addition, from mid-October to mid-November, air masses influenced by crop residue burning and containing soot particles affect the sampling site. The presence of element V could also indicate contributions from industrial combustion processes, particularly oil refining and coal burning. The presence of Sr may be linked to fertilizer application. Furthermore, the strong association with FI implies the contribution of dissolved organic matter with microbial or terrestrial origin. Factor 4 has a major contribution from Mn, Co, Cu, Cd and Pb, indicating an association with agricultural activities (e.g., soil dust and fertilizer use) and industrial processes.

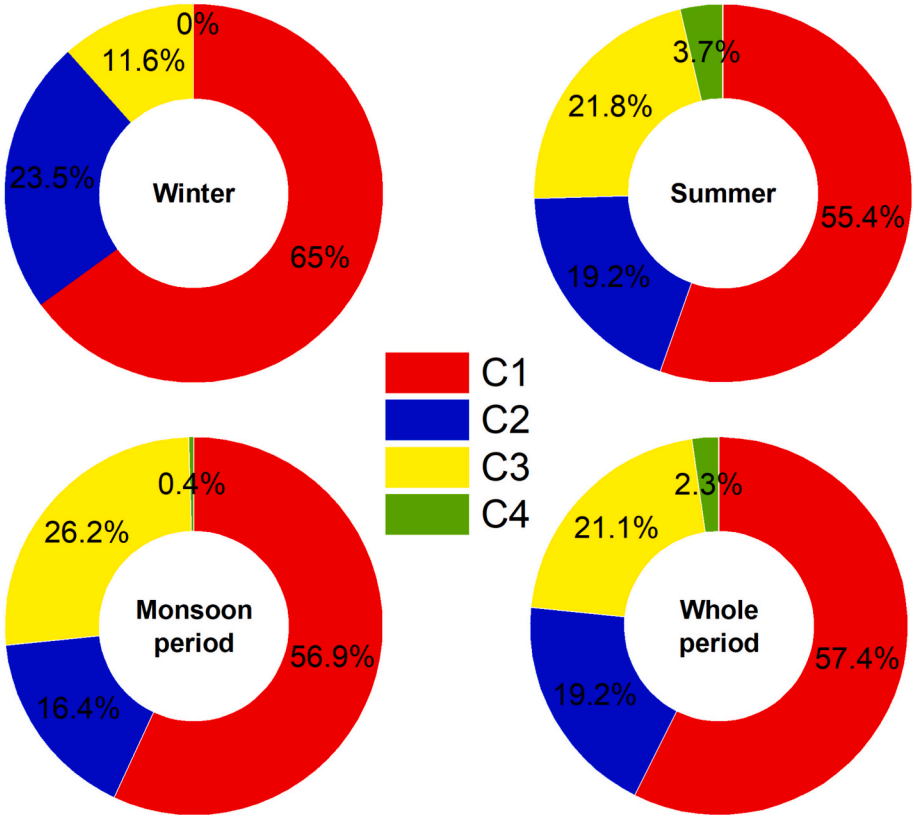

Fig. 7. Relative contributions of 4 PARAFAC-derived chromophore components for $PM_{2.5}$ and PM_{10} in Ajmer during different sampling periods.

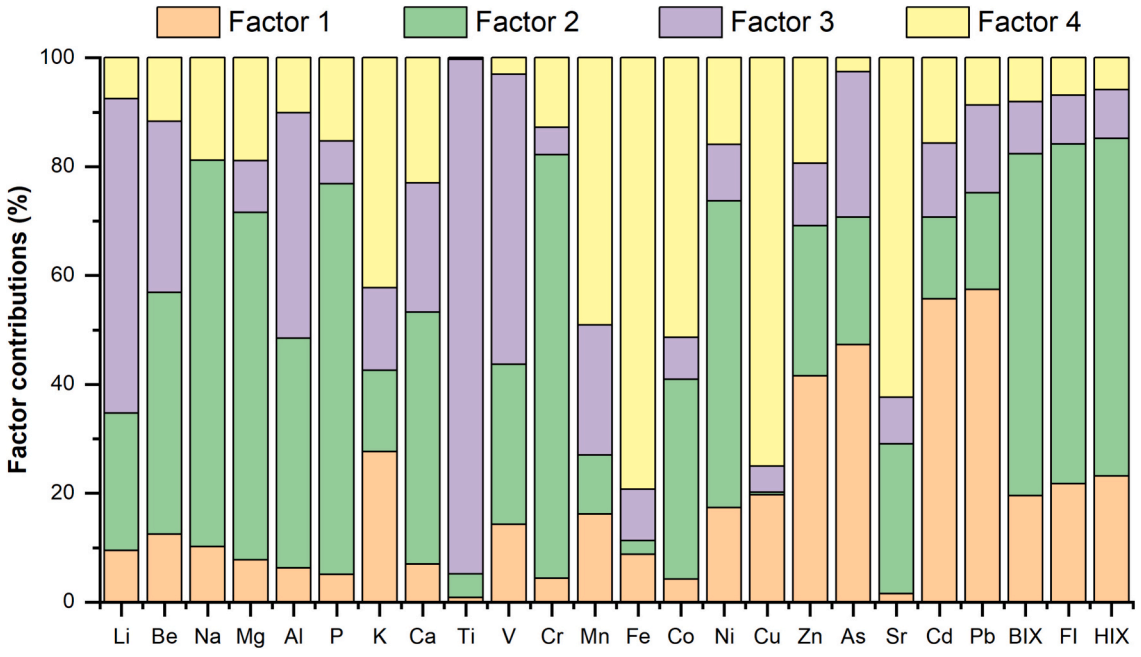

Fig. 8. Source apportionment of elements and EEM fluorescence indices using the PMF model in Karlsruhe, Germany.

4. Limitations

While this study provides valuable insights into $PM_{2.5}$ and PM_{10} characteristics in Karlsruhe and Ajmer, several limitations should be acknowledged. Sampling was conducted at single fixed sites in each city, which may not fully capture the spatial variability of $PM_{2.5}$ and PM_{10} composition and sources across different urban zones such as industrial, residential, or background areas. The sampling periods were not concurrent (Karlsruhe: July 2021–October 2022; Ajmer: January–June 2023), limiting direct season-by-season comparisons, and the smaller dataset for Ajmer, particularly for elemental analysis ($n = 16$), may reduce the robustness of statistical comparisons and trend analyses.

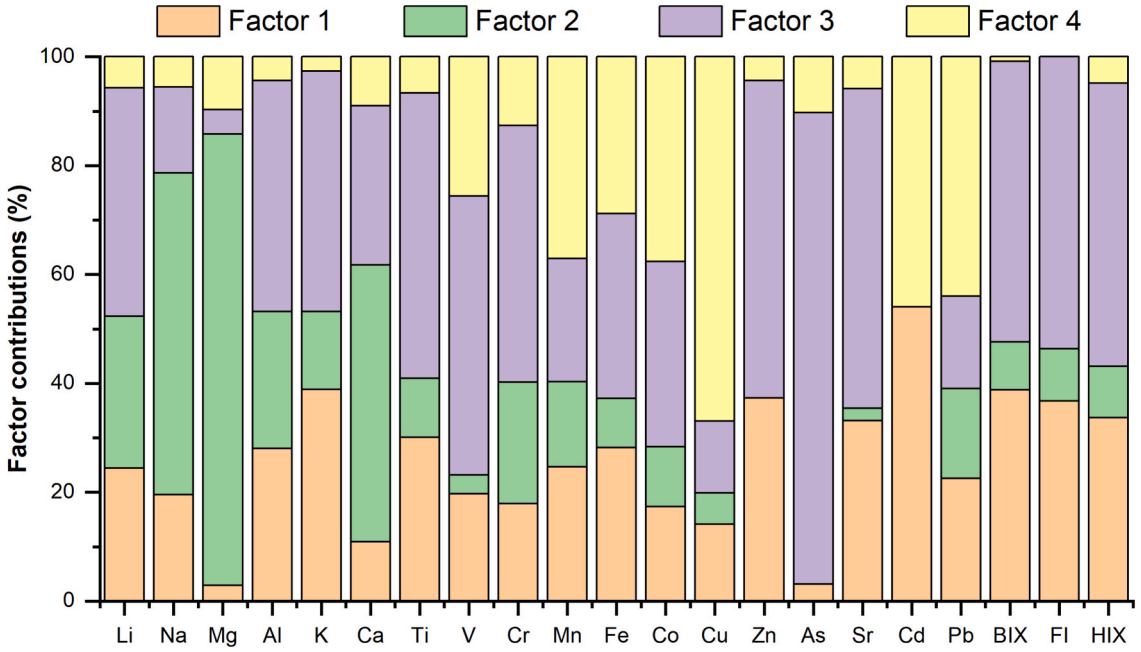

Fig. 9. Source apportionment of elements and EEM fluorescence indices using PMF model in Ajmer, India.

Nevertheless, these samples for ICP-MS analysis were carefully selected to represent the major temporal variations throughout the sampling period, providing sufficient information to reliably identify and apportion the primary PM sources. It should be noted that source interpretation based on individual diagnostic ratios or chemical markers is inherently limited, as such indicators may be influenced by multiple sources and atmospheric processes. Furthermore, fluorescence spectroscopy characterizes water-soluble organic carbon but provides limited information on total or insoluble organic fractions; using alternative extraction solvents, such as methanol, could help capture additional organic chromophores information in PM. Although multiple chemical indicators were jointly considered in this study, uncertainties remain. Future studies could further strengthen source tracing by integrating multiple complementary approaches, such as aerosol size distribution, isotopic analysis, and high-time-resolution measurements.

5. Conclusion

This study analyzes the cross-regional characteristics, chemical composition, and sources of atmospheric particulate matters in Karlsruhe, Germany, and Ajmer, India. By integrating ICP-MS elemental analysis, 3D-EEM, fluorescence indices, and PMF modeling, the study successfully identified and apportioned the key PMs sources in these contrasting urban environments.

In Karlsruhe, $PM_{2.5}$ and PM_{10} were primarily influenced by traffic-related non-exhaust emissions (indicated by elevated Cu/Zn ratios), industrial activities (reflected by Zn, As, Cd, Pb, and specific fluorescent components), and seasonal biomass combustion (supported by the variation of less-oxygenated HULIS component, C3). Fluorescent organic aerosols were dominated by highly oxygenated HULIS component, suggesting substantial secondary formation influenced by anthropogenic precursors from the industrial infrastructure.

In contrast, PMs in Ajmer were mainly affected by crustal and desert dust sources, Copper and Zinc mining, as evidenced by higher concentrations of Na, Al, and Ca, along with lower Fe/Al and Ti/Al ratios. Biomass burning, including domestic fuel and coal combustion, was a significant contributor, indicated by the dominance of less-oxygenated HULIS components in fluorescence analysis. PMF results, combined with lower V/Pb ratios and specific elemental associations, further highlighted contributions from industrial emissions and mixed combustion sources.

Overall, the study demonstrates that PMs sources and composition vary markedly between temperate European and arid Indian urban environments, reflecting differences in climate, geography, and anthropogenic activities. These findings provide critical insights into the source-specific characteristics of urban aerosols and can inform targeted air quality management strategies in diverse urban settings.

CRediT authorship contribution statement

Xiao Wang: Writing – review & editing, Writing – original draft, Visualization, Methodology, Formal analysis, Data curation, Conceptualization. **Ramesh P. Singh:** Writing – review & editing, Resources, Methodology, Data curation. **Elisabeth Eiche:** Writing – review & editing, Resources, Methodology, Data curation. **Feng Jiang:** Writing – review & editing, Software, Methodology, Data curation. **Prity S. Pippal:** Writing – review & editing, Resources, Data curation. **Rajesh Kumar:** Writing – review & editing, Resources, Data curation. **Akshansha Chauhan:** Writing – review & editing, Resources, Data curation. **Stefan Norra:** Writing – review & editing, Supervision, Resources, Project administration, Methodology, Funding acquisition.

Declaration of competing interest

The authors declare that they have no known competing financial interests or personal relationships that could have appeared to influence the work reported in this paper.

Acknowledgments

We would like to thank Nadine Hüll, Maya Denker and Chantalle Kotschenreuther at Karlsruhe Institute of Technology (KIT) for their assistance with sample preparation and analysis. Xiao Wang gratefully acknowledges financial support from the China Scholarship Council (CSC) with project number CSC202106400009. The authors are grateful to the anonymous reviewers for providing useful comments/suggestions that have helped us to improve earlier versions of the manuscript. Ramesh Singh spent three months at the University of Potsdam, Golm,

Germany, he is grateful to the Alexander von Humboldt Foundation for sponsoring his visit.

Appendix A. Supplementary data

Supplementary data to this article can be found online at https://doi.org/10.1016/j.scitotenv.2026.181386.

Data availability

Data will be made available on request.

References

Aryal, R., Lee, B.K., Beecham, S., Kandasamy, J., Aryal, N., Parajuli, K., 2015. Characterisation of road dust organic matter as a function of particle size: a PARAFAC approach. Water Air Soil Pollut. 226 (2), 24. https://doi.org/10.1007/s11270-014-2289-y.

Cao, T., Li, M.J., Xu, C.C., Song, J.Z., Fan, X.J., Li, J., 2023. Technical note: chemical composition and source identification of fluorescent components in atmospheric water-soluble brown carbon by excitation–emission matrix spectroscopy with parallel factor analysis – potential limitations and applications. Atmos. Chem. Phys. 23, 2613–2625. https://doi.org/10.5194/acp-23-2613-2023.

Chen, Q., Li, J.W., Hua, X.Y., Jiang, X.T., Mu, Z., Wang, M.M., et al., 2020. Identification of species and sources of atmospheric chromophores by fluorescence excitation-emission matrix with parallel factor analysis. Sci. Total Environ. 718, 137322. https://doi.org/10.1016/j.scitotenv.2020.137322.

Chen, Q., Miyazaki, Y., Kawamura, K., Matsumoto, K., Coburn, S., Volkamer, R., et al., 2016a. Characterization of chromophoric water-soluble organic matter in urban, forest, and marine aerosols by HR-ToF-AMS analysis and excitation-emission matrix spectroscopy. Environ. Sci. Technol. 50 (19), 10351–10360. https://doi.org/10.1021/acs.est.6b01643.

Chen, W., Zhang, M., Liu, W., Fu, J., Guo, L., 2022. Real-time source apportionment of $PM_{2.5}$ highlights the importance of joint controls on atmospheric pollution in cold region of China. Remote Sens. 14 (15), 3770. https://doi.org/10.3390/rs14153770.

Chen, Y., Schleicher., N.J., Fricker, M., Cen, K., Liu, X., Kaminski, U., et al., 2016b. Long-term variation of black carbon and $PM_{2.5}$ in Beijing, China with respect to meteorological conditions and governmental measures. Environ. Pollut. 212, 269–278. https://doi.org/10.1016/j.envpol.2016.01.008.

Das, R., Mohtar, A.T.B.M., Rakshit, D., Shome, D., Wang, X., 2018. Sources of atmospheric lead (Pb) in and around an Indian megacity. Atmos. Environ. 193, 57–65. https://doi.org/10.1016/j.atmosenv.2018.08.062.

Dey, S., Mukherjee, A., Polana, A.J., Rana, A., Mao, J.Y., Jia, S.G., et al., 2021. Brown carbon aerosols in the indo-Gangetic plain outflow: insights from excitation emission matrix (EEM) fluorescence spectroscopy. Environ. Sci. Process Impacts 23, 745–755. https://doi.org/10.1039/d1em00050k.

Dey, S., Tripathi, S.N., Singh, R.P., Holben, B.N., 2004. Influence of dust storms on the aerosol optical properties over the indo-Gangetic basin. J. Geophys. Res. 109, D20211. https://doi.org/10.1029/2004JD004924.

Dong, Z.C., Pavuluri, C.M., Li, P.S., Xu, Z.J., Deng, J.J., Zhao, X.Y., et al., 2024. Measurement report: optical characterization, seasonality, and sources of brown carbon in fine aerosols from Tianjin, North China: year-round observations. Atmos. Chem. Phys. 24 (10), 5887–5905. https://doi.org/10.5194/acp-24-5887-2024.

Fu, P., Mostofa, K.M.G., Wu, F., Liu, C., Li, W., Liao, H., et al., 2010. Excitation-emission matrix characterization of dissolved organic matter sources in two eutrophic lakes (southwestern China plateau). Geochem. J. 44, 99–112. https://doi.org/10.2343/geochemj.1.0047.

Fuzzi, S., Baltensperger, U., Carslaw, K., Decesari, S., Denier van der Gon, H., Facchini, M.C., et al., 2015. Particulate matter, air quality and climate: lessons learned and future needs. Atmos. Chem. Phys. 15 (14), 8217–8299. https://doi.org/10.5194/acp-15-8217-2015.

Hansen, A.M., Kraus, T.E.C., Pellerin, B.A., Fleck, J.A., Downing, B.D., Bergamaschi, B.A., 2016. Optical properties of dissolved organic matter (DOM): effects of biological and photolytic degradation. Limnol. Oceanogr. 61, 1015–1032. https://doi.org/10.1002/lno.10270.

Hird, C., Perron, M.M.G., Holmes, T.M., Meyerink, S., Nielsen, C., Townsend, A.T., et al., 2024. On the use of lithogenic tracer measurements in aerosols to constrain dust deposition fluxes to the ocean southeast of Australia. Aerosol Res. 2, 315–327. https://doi.org/10.5194/ar-2-315-2024.

Huguet, A., Vacher, L., Relexans, S., Saubusse, S., Froidefond, J.M., Parlanti, E., 2009. Properties of fluorescent dissolved organic matter in the Gironde estuary. Org. Geochem. 40, 706–719. https://doi.org/10.1016/j.orggeochem.2009.03.002.

Jain, R., Bhu, H., Kumar, H., Purohit, R., 2022. Integration of multi-sensor remote sensing, geological and geochemical data for delineation of Pb–Zn bearing carbonates of Middle Aravalli group in Zawar–Dungarpur Belt. NW India. Geocarto Int. 37 (27), 17165–17199. https://doi.org/10.1080/10106049.2022.2123958.

Jeong, H., Lee, S., Kim, J., 2022. Characteristics of potentially toxic elements and multi-isotopic signatures in atmospheric particulate matter from urban environments. Environ. Pollut. 276, 118339. https://doi.org/10.1016/j.envpol.2021.118339.

Jiang, F., Song, J., Bauer, J., Gao, L., Vallon, M., Gebhardt, R., et al., 2022. Chromophores and chemical composition of brown carbon characterized at an urban kerbside by excitation–emission spectroscopy and mass spectrometry. Atmos. Chem. Phys. 22, 14971–14986. https://doi.org/10.5194/acp-22-14971-2022.

Jiang, W.M., Smyth, S., Giroux, É., Roth, H., Yin, D.Z., 2006. Differences between CMAQ fine mode particle and PM2.5 concentrations and their impact on model performance evaluation in the lower Fraser valley. Atmos. Environ. 40, 4973–4985. https://doi.org/10.1016/j.atmosenv.2005.10.069.

Kaskaoutis, D.G., Gautam, R., Singh, R.P., Houssos, E.E., Goto, D., Singh, S., et al., 2012. Influence of anomalous dry conditions on aerosols over India: transport, distribution and properties. J. Geophys. Res. Atmos. 117, D09106. https://doi.org/10.1029/2011JD017314.

Kumar, V., Sahu, M., Biswal, B., Prakash, J., Choudhary, S., Raliya, R., et al., 2024. Real-time source apportionment of particulate matter from low-cost particle sensors using machine learning. Aerosol Sci. Eng. 1-11. https://doi.org/10.1007/s41810-024-00271-3.

Lee, H.J., Laskin, A., Laskin, J., Nizkorodov, S.A., 2013. Excitation–emission spectra and fluorescence quantum yields for fresh and aged biogenic secondary organic aerosols. Environ. Sci. Technol. 47, 5763–5770. https://doi.org/10.1021/es400644c.

Ma, L.X., Li, Z., Li, B., Fu, D.L., Sun, X.Z., Sun, S.J., et al., 2022. Light-absorption and fluorescence fingerprinting characteristics of water and methanol soluble organic compounds in $PM_{2.5}$ in cold regions of Northeast China. Sci. Total Environ. 832, 155081. https://doi.org/10.1016/j.scitotenv.2022.155081.

Murphy, K.R., Stedmon, C.A., Graeber, D., Bro, R., 2013. Fluorescence spectroscopy and multi-way techniques. PARAFAC. Anal. Methods 5, 6557–6566. https://doi.org/10.1039/C3AY41160E.

Prasad, A.K., Singh, R.P., Kafatos, M., 2006. Influence of coal based thermal power plants on aerosol optical properties in the indo-Gangetic basin. Geophys. Res. Lett. 33, L05805. https://doi.org/10.1029/2005GL023801.

Pucher, M., Wünsch, U., Weigelhofer, G., Murphy, K., Hein, T., Graeber, D., 2019. staRdom: versatile software for analyzing spectroscopic data of dissolved organic matter in R. Water 11 (11), 2366. https://doi.org/10.3390/w11112366.

Rai, P., Furger, M., El Haddad, I., Kumar, V., Wang, L.W., Singh, A., et al., 2020. Real-time measurement and source apportionment of elements in Delhi's atmosphere. Sci. Total Environ. 742, 140332. https://doi.org/10.1016/j.scitotenv.2020.140332.

Ray, I., Mitra, S., Kayee, J., Yuan, S.F., Nagendra, S.S., Wang, X.F., Das, R., 2024. Dominance of open burning signatures in $PM_{2.5}$ near coal plant should redefine pollutant priorities of India. npj Clim. Atmos. Sci. 7 (1), 284. https://doi.org/10.1038/s41612-024-00836-6.

Rutherford, J.W., Dawson-Elli, N., Manicone, A.M., Korshin, G.V., Novosselov, I.V., Seto, E., Posner, J.D., 2020. Excitation emission matrix fluorescence spectroscopy for combustion generated particulate matter source identification. Atmos. Environ. 220, 117065. https://doi.org/10.1016/j.atmosenv.2019.117065.

Rutherford, J.W., Larson, T.V., Gould, T., Seto, E., Novosselov, I.V., Posner, J.D., 2021. Source apportionment of environmental combustion sources using excitation emission matrix fluorescence spectroscopy and machine learning. Atmos. Environ. 259, 118501. https://doi.org/10.1016/j.atmosenv.2021.118501.

Sciscenko, I., Arques, A., Micó, P., Mora, M., García-Ballesteros, S., 2022. Emerging applications of EEM-PARAFAC for water treatment: a concise review. Chem. Eng. J. Adv. 10, 100286. https://doi.org/10.1016/j.ceja.2022.100286.

Sharma, M., 2020. Air Quality Assessment, Trend Analysis, Emission Inventory and Source Apportionment Study in Jaipur City. https://environment.rajasthan.gov.in/content/dam/environment/RPCB/EnvironmentalReport/Final-Report-Source-Apportionmnent-Study-Jaipur-IITKanpur.pdf.

Sharma, S.K., Mandal, T.K., 2023. Elemental composition and sources of fine particulate matter ($PM_{2.5}$) in Delhi, India. Bull. Environ. Contam. Toxicol. 110, 60. https://doi.org/10.1007/s00128-023-03707-7.

Shelley, R.U., Morton, P.L., Landing, W.M., 2015. Elemental ratios and enrichment factors in aerosols from the US GEOTRACES North Atlantic transects. Bull. Environ. Contam. Toxicol. 116, 262–272. https://doi.org/10.1016/j.dsr2.2014.12.005.

Singh, R.P., Prasad, A.K., Kayetha, V.K., Kafatos, M., 2008. Enhancement of oceanic parameters associated with dust storms using satellite data. J. Geophys. Res. 113, C11008. https://doi.org/10.1029/2008JC004815.

Siudek, P., 2024. Chemical composition and source apportionment of ambient $PM_{2.5}$ in a coastal urban area, northern Poland. Chemosphere 356, 141850. https://doi.org/10.1016/j.chemosphere.2024.141850.

Taylor, S.R., McLennan, S.M., 1985. The Continental Crust: Its Composition and Evolution Blackwell. Oxford.

Tuladhar, A., Manandhar, P., Shrestha, K.L., 2021. Assessment of health impact of $PM_{2.5}$ exposure by using WRF-Chem model in Kathmandu Valley. Nepal. Front. Sustain. Cities 3, 672428. https://doi.org/10.3389/frsc.2021.672428.

Viana, M., Kuhlbusch, T.A.J., Querol, X., Alastuey, A., Harrison, R.M., Hopke, P.K., et al., 2008. Source apportionment of particulate matter in Europe: a review of methods and results. Aerosol Sci. 39, 827e849. https://doi.org/10.1016/j.jaerosci.2008.05.007.

Wang, Y., Wang, Y., Lu, X., Sun, W., Xu, Y., Zhou, J., Sun, Y., 2022. Catalytic ozonation for effective degradation of coal chemical biochemical tail water by Mn/Ce@ RM catalyst. Water 14 (2), 206. https://doi.org/10.3390/w14020206.

Wedepohl, K.H., 1995. The composition of the continental crust. Geochim. Cosmochim. Acta 59 (7), 1217–1232. https://doi.org/10.1016/0016-7037(95)00038-2.

Wu, B., Dai, X., Chai, X., 2017. Simultaneous enhancement of sludge dewaterability and removal of sludge-borne heavy metals through a novel oxidative leaching induced by nano-CaO_2. Environ. Sci. Pollut. Res. 24, 16263–16275. https://doi.org/10.1007/s11356-017-9261-5.

Wu, G., Ram, K., Fu, P., Wang, W., Zhang, Y., Liu, X., et al., 2019. Water-soluble brown carbon in atmospheric aerosols from Godavari (Nepal), a regional representative of South Asia. Environ. Sci. Technol. 53 (7), 3471–3479. https://doi.org/10.1021/acs.est.9b00596.

Xu, X., Kang, J., Shen, J., Zhao, S., Wang, B., Zhang, X., Chen, Z., 2021. EEM–PARAFAC characterization of dissolved organic matter and its relationship with disinfection by-products formation potential in drinking water sources of northeastern China. Sci. Total Environ. 774, 145297. https://doi.org/10.1016/j.scitotenv.2021.145297.

Yadav, V., Rajamani, V., 2005. Air quality and trace metal chemistry of different size fractions of aerosols in N–NW India—implications for source diversity. Atmos. Environ. 40 (4), 698–712. https://doi.org/10.1016/j.atmosenv.2005.10.00.

Zhang, C., Jing, D., Wu, C., Li, S., Cheng, N., Li, W., et al., 2021. Integrating chemical mass balance and the community multiscale air quality models for source identification and apportionment of $PM_{2.5}$. Process. Saf. Environ. Prot. 149, 665–675. https://doi.org/10.1016/j.psep.2021.03.033.

Zhang, G., Ding, C., Jiang, X., Pan, G., Wei, X., Sun, Y., 2020. Chemical compositions and sources contribution of atmospheric particles at a typical steel industrial urban site. Sci. Rep. 10, 7654. https://doi.org/10.1038/s41598-020-64519-x.